Chaos

Abrupt and gradual onset of synchronized oscillations due to dynamical quorum sensing in the single-cathode multi-anode nickel electrodissolution system

Cite as: Chaos **29**, 033114 (2019); https://doi.org/10.1063/1.5087405
Submitted: 31 December 2018 . Accepted: 19 February 2019 . Published Online: 07 March 2019

Michael J. Hankins, Vilmos Gáspár, and István Z. Kiss

View Online Export Citation CrossMark

ARTICLES YOU MAY BE INTERESTED IN

Prediction of robust chaos in micro and nanoresonators under two-frequency excitation
Chaos: An Interdisciplinary Journal of Nonlinear Science **29**, 033112 (2019); https://doi.org/10.1063/1.5058750

Hierarchical transitions in multiplex adaptive networks of oscillatory units
Chaos: An Interdisciplinary Journal of Nonlinear Science **28**, 121101 (2018); https://doi.org/10.1063/1.5077075

Robustness of partially interdependent networks under combined attack
Chaos: An Interdisciplinary Journal of Nonlinear Science **29**, 021101 (2019); https://doi.org/10.1063/1.5085850

AIP Publishing

© 2019 Author(s).

Abrupt and gradual onset of synchronized oscillations due to dynamical quorum sensing in the single-cathode multi-anode nickel electrodissolution system

Cite as: Chaos **29**, 033114 (2019); doi: 10.1063/1.5087405
Submitted: 31 December 2018 · Accepted: 19 February 2019 ·
Published Online: 7 March 2019

View Online Export Citation CrossMark

Michael J. Hankins,[1,2] Vilmos Gáspár,[3] and István Z. Kiss[1]

AFFILIATIONS

[1]Department of Chemistry, Saint Louis University, St. Louis, Missouri 63103, USA
[2]Department of Chemistry, Southern Illinois University Edwardsville, Edwardsville, Illinois 62026, USA
[3]Laboratory of Nonlinear Chemical Dynamics, Institute of Chemistry, Eötvös Loránd University, Pázmány P. sétány 1/A, Budapest 1117, Hungary

Note: This paper is part of the Focus Issue, "Nonlinear Chemical Dynamics and Its Interdisciplinary Impact: Dedicated to Ken Showalter on the Occasion of his 70th Birthday."

ABSTRACT

The nonlinear dynamics of an oscillatory Ni electrodissolution–hydrogen ion reduction system are explored in a multi-electrode anode–single cathode system. A mathematical analysis of the charge balance equations reveals that the coupling scheme is similar to dynamical quorum sensing, where the number of anode wires affects a parameter related to the population density. In a parameter region where the large population exhibits stationary behavior, with sufficiently strong coupling (with small individual resistances attached to the anode wires), synchronized oscillations emerge abruptly with decreasing the number of anodes. Therefore, an "inverse" dynamical quorum sensing takes place. With weak coupling the transition is gradual. The experiments are supported by numerical simulation of a kinetic model of the process. The results thus show that the description of nontrivial cathode-anode interactions in the form of dynamical quorum sensing provides an efficient way of analyzing the dynamical response of complex, interacting electrochemical reactions.

Published under license by AIP Publishing. https://doi.org/10.1063/1.5087405

Bacteria can sense the population density through quorum sensing: Each cell can secrete autoinducer molecules, which are then mixed in the intercellular medium. The bacteria can detect the intercellular concentration of the autoinducer molecules (with receptors), which depends on the population density. Therefore, the bacteria can determine the population density and orchestrate a coordinated behavior. For survival, it is essential to design population density dependent processes. We analyze a seemingly different *abiotic* process: The behavior of an electrochemical reaction where the electrons produced by the anode are consumed by the cathode. When this process takes place in a particular configuration with multiple anodes and a single cathode, a mathematical analysis shows that the underlying kinetic equations are equivalent to dynamical quorum sensing. We show that the electrochemical cell can generate population density dependent oscillations and synchronization through the inherent quorum sensing coupling scheme.

I. INTRODUCTION

Synchronization of rhythmic activity plays a vital role in the functioning of biological systems.[1,2] With population of oscillators, global interactions (all-to-all coupling) can induce a transition to synchronization.[1,3] Such interactions can occur through global constraints,[4,5] feedback,[6] or a common media with a coupling factor.[7,8] Bacteria, for example, use the autoinducer molecule concentration in the intercellular medium to determine their own population density in order to regulate gene expression.[9] This phenomenon is known as quorum sensing. Some bacterial gene expressions occur only at a high cell-population density in response to the accumulation of secreted autoinducer signaling molecules. A "quorum" of bacteria is needed to effectively produce the desired effect of the gene expression. For certain deep sea marine life, bacterial gene expression of *Vibrio fischeri* causes bioluminescence.[10,11] In *Escherichia coli*,

Published under license by AIP Publishing.

the gene expression causes virulence in the host body.[12,13] Quorum sensing can provide the mechanism for modulation of immune system response,[14] biofilm detachment,[15] or "flocking" of swimming bacteria.[16]

The emergence of oscillatory glucose metabolism at sufficiently high yeast cell density[17] inspired the design of well-controlled experiments[18–20] and related modeling[21–23] to clarify the dynamical mechanism of the complex process. A general dynamical model, based on repressilator oscillators coupled through a well-mixed intercellular media, showed that the cellular oscillations can exhibit robust synchronization.[21] The Showalter group designed an experimental system with Belousov-Zhabotinsky (BZ) beads, where the oscillations occurred on the surface of the beads, and the coupling took place through the well-stirred solution.[7,24,25] Depending on the stirring (exchange) rate, gradual or sudden onset of the synchronized oscillatory activity was observed with the increase of the oscillator (BZ bead) density.[7] Coupling through an inactive medium found applications in various systems through "crowd synchrony" and was applied to the coherent oscillations of the Millenium Bridge,[26] lasers,[27] circuits,[28,29] the mercury drop ("beating heart") chemomechanical oscillator system,[30] and synchronized synthetic biological clocks.[31]

Electrochemical oscillators exhibit rich synchronization dynamics that include Kuramoto transitions,[4] stable[32,33] and itinerant[34] cluster states, and chimera patterns.[35,36] These studies were performed in the traditional "three-electrode" configuration with a reference, a counter, and an electrode array as the working electrode. The coupling among the working electrodes typically occurs through the traditional ("direct") coupling scheme, e.g., through an external resistance interface,[4,36] potential drops in the electrolyte,[37] or external feedback.[34] However, in many practical applications (e.g., fuel cells), a "two-electrode" configuration is used with a cathode and an anode that are connected. In a previous publication,[38] the coupling of nickel electrodissolution and hydrogen ion reduction resulted in oscillations under conditions where none of the electrodes could display instabilities. With two nickel wires as anode under oscillatory conditions, the cathode surface area could be adjusted such that the oscillations became synchronized.[39]

In this paper, motivated by the methodology of the quorum sensing "crowd synchrony" experiments, we investigate the effect of the number of anode wires on the emergence of oscillations and synchronization in a multi-particle anode and single-cathode electrochemical cell. The experiments are performed in a "two-electrode" cell with nickel wires (anode) and a nickel plate (cathode) in the sulfuric acid electrolyte; the fraction of the oscillatory (vs. stationary) dissolution and the synchronized (vs. desynchronized) elements are analyzed as a function of the number of the anode wires (1-40), while keeping all other parameters fixed. A kinetic model is formulated based on mass and charge balance in the cell. A comparison is made between the model structure of the electrochemical process and that of the general dynamical quorum sensing model. The features of the onset of oscillations and synchronization by changing the number of the anode wires ("population density") are compared with strong and weak coupling, by tuning the individual resistance attached to the anode wires. The experiments are supported by numerical simulations.

II. BACKGROUND

The reported results in this Focus Issue on Nonlinear Chemical Dynamics and Its Interdisciplinary Impact—like many of our research papers published during the last 25 years—are closely related to the seminal contributions of Kenneth Showalter to the field. It is true in spite of the fact that while Showalter studied temporal and spatial-temporal instabilities (oscillations, chaos, synchronization, quorum sensing, chimeras, chemical waves, pattern formation, etc.) in homogeneous and reaction-diffusion chemical systems, our research focused on the same dynamical phenomena occurring in electrochemical systems. Interestingly, the origin of our decision to initiate research in this old subfield of oscillating phenomena (the first electrochemical oscillator was reported in 1828[40]) also stems from the groundbreaking research of Showalter *et al.* Between 1986 and 1993, Vilmos Gáspár (one of the authors of this paper) had the privilege to work as a postdoctoral research fellow in the group of Kenneth Showalter at West Virginia University. Certainly, one of the major contributions of the group to the development of the field was the report on the experimental control of chemical chaos in the Belousov-Zhabotinsky (BZ) reaction.[41] That series of experiments required eight-hour shift work of the group (Valery, Jonathan, and Vilmos) for many weeks in order to maintain the operation of the so-called the continuous, stirred, flow-through tank reactor (CSTR); hundreds of liters of solutions of well-defined concentrations of the reactants were consumed, zillions of data were stored and analyzed in order to construct the chaotic attractor, create the Poincaré section, and apply the proportional feedback control algorithm. Returning to Debrecen (Hungary) in 1993, V.G. found and teamed up with a new undergraduate student István Z. Kiss (he later also worked in the group toward his Ph.D.). He was very much interested in the field, and, together, we built a computer controlled electrochemical workstation for chaos control. Our original goal was to study chaotic dynamics, develop and test different control algorithms, etc., by using electrochemical systems, in which the period of oscillations is shorter and data can be collected easier. We reported our successful experiments in 1997.[42] These experiments were then followed by many others expanding our field of interest toward more complex phenomena, e.g., control of synchronization.[43] Now, we report on results related to the onset of synchronization in an electrochemical system due to coupling similar to the quorum sensing mechanism studied by Showalter and co-workers.[7]

III. EXPERIMENTAL SETUP

The electrochemical cell was constructed using a 250 ml water-jacketed beaker connected to a Thermo Scientific Neslab RTE 7 circulating bath. The electrolyte was 3M sulfuric acid (Macron). The 6 cm^2 surface area nickel cathode plate was made from 99+% 0.05 mm thick annealed nickel foil (Alfa Aesar). (Previous study[39] established that about 0.5 cm^2 surface area cathode/anode wire provides strong coupling in the system. With very large cathode the coupling would be very weak; with very small electrode hydrogen bubble formation can block the electrode, and cause reproducibility issues. The chosen cathode size thus supports strong coupling for about 12 anode wires.) The anode was an electrode array made from forty 1.0 mm diameter nickel wires (99.98%, Goodfellow); the wires were embedded in Armstrong C-7 epoxy resin so that only the cross-sections of the wires

Published under license by AIP Publishing.

were exposed to the solution. The surfaces of these electrodes were polished using Buehler polishing pads (P120 to P4000). The cathode plate (counter and reference electrode) and the anode electrode array (working electrode) were connected to a potentiostat (Pine AFCBP1); the potentiostat applied a constant circuit potential (V) in a "two-electrode" configuration. The currents of the anodes were collected with multichannel ammeters. To observe oscillatory behavior, individual resistances ($R_{\text{ind}} = 2.5\,\text{k}\Omega$, $5\,\text{k}\Omega$, or $10\,\text{k}\Omega$) were inserted between the nickel wires and the working point of the potentiostat.

The experimental setup and the circuit diagram of the cathode-anode configuration are shown in Fig. 1. The cathodic and anodic reactions (hydrogen ion reduction and nickel electrodissolution, respectively) take place on the electrode surfaces, which share the common sulfuric acid electrolyte.

IV. RESULTS AND DISCUSSION

A. Experiments

In the experiments, the effect of the number of the anode wires is explored on the emergence of oscillations and their synchronization at the fixed circuit potential and individual resistance.

The experiments were performed by connecting all the $N = 40$ nickel anode wires and increasing the circuit potential just before the oscillations occur (through a Hopf bifurcation[44]) in the presence of the attached individual resistances. The circuit potential was then kept constant, and the anode wires were disconnected one at a time. The current vs. time behavior was recorded after the removal of each electrode.

Figure 2(a) shows the current vs. time at the beginning of the experiments at $N = 40$ with relatively small individual resistance ($R_{ind} = 2.5\,\text{k}\Omega$). The current signal is stationary at a mean value of about 0.095 mA. The small differences in the electrode currents are related to the inherent heterogeneities in the experiments, e.g., due to differing surface conditions.[45] As the number of electrodes were decreased, the system exhibited transition to the oscillatory state where current oscillations could be observed on a fraction of the connected elements [Fig. 3(a)] and some of these oscillations could be (frequency) synchronized [Fig. 3(d)]. As it is shown in Figs. 3(a) and 3(d), when the number of electrodes were decreased from $N = 15$ to $N = 14$, there was an abrupt transition where the currents of all the connected electrodes exhibited fully synchronized oscillations. This synchronized oscillatory state is shown in Fig. 2(b) ($N = 14$). The sudden change of dynamics by decreasing the number of oscillators, with the emergence of synchronized oscillation, can be considered as a dynamical quorum transition. We note that in many studies, the oscillation rises with an increase in the population density;[18,24] in the electrochemical example, the oscillatory transition occurs with decreasing the number of anodes (and thus the quantity related to population density), therefore, we consider the process as an "inverse" dynamical transition mediated by quorum sensing.

When a higher individual resistance was used, the transition to an oscillatory state did not occur at the same N for all electrodes. At $R_{ind} = 10\,\text{k}\Omega$ with $N = 40$, the anodes exhibit stationary currents; when N is decreased to 30, one of the electrodes exhibits large amplitude oscillations, and the rest stationary behavior [see Fig. 2(c)]. As the anode wires are further removed, the transition resembled that of a progressive (or gradual) onset of oscillations and synchronization. As shown in Figs. 3(c) and 3(f), the system is not fully oscillatory until $N = 7$, and not fully synchronized until $N = 5$. Figure 2(d) shows the typical behavior that consists of mixed (nearly) stationary and oscillatory, synchronized and desynchronized oscillations with $N = 11$.

At an intermediate resistance ($R_{\text{ind}} = 5\,\text{k}\Omega$), the abruptness of the transition to oscillations and synchronization is in between what

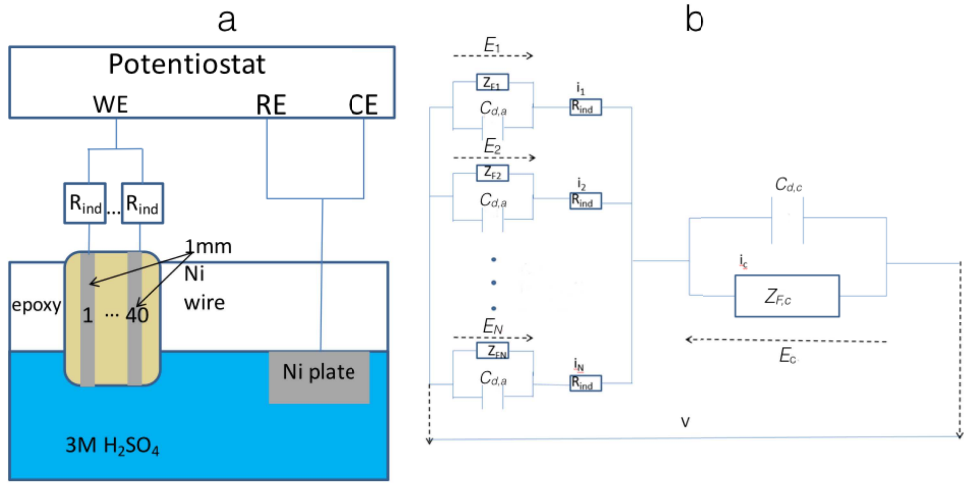

FIG. 1. Schematic of the "two-electrode" electrochemical cell with multiple anodes connected to a single cathode. (a) Experimental setup using nickel wire anodes (working electrode) and a nickel plate cathode (counter and reference electrodes). (b) Equivalent circuit. Electrolyte: 3M H_2SO_4 at 10.0 °C. WE, working electrode; CE, counter electrode; RE, reference electrode; R_{ind}, individual resistance. Z_{Fk}, i_k, E_k ($k = 1,2,\ldots,N$) are the Faradaic impedance, current, and the electrode potential of the k-th anode, respectively. $C_{d,a}$ and $C_{d,c}$ are the anodic and cathodic double layer capacitances, respectively. $Z_{F,c}$, i_c, and E_c are the cathodic Faradaic impedance, current, and electrode potential, respectively.

Published under license by AIP Publishing.

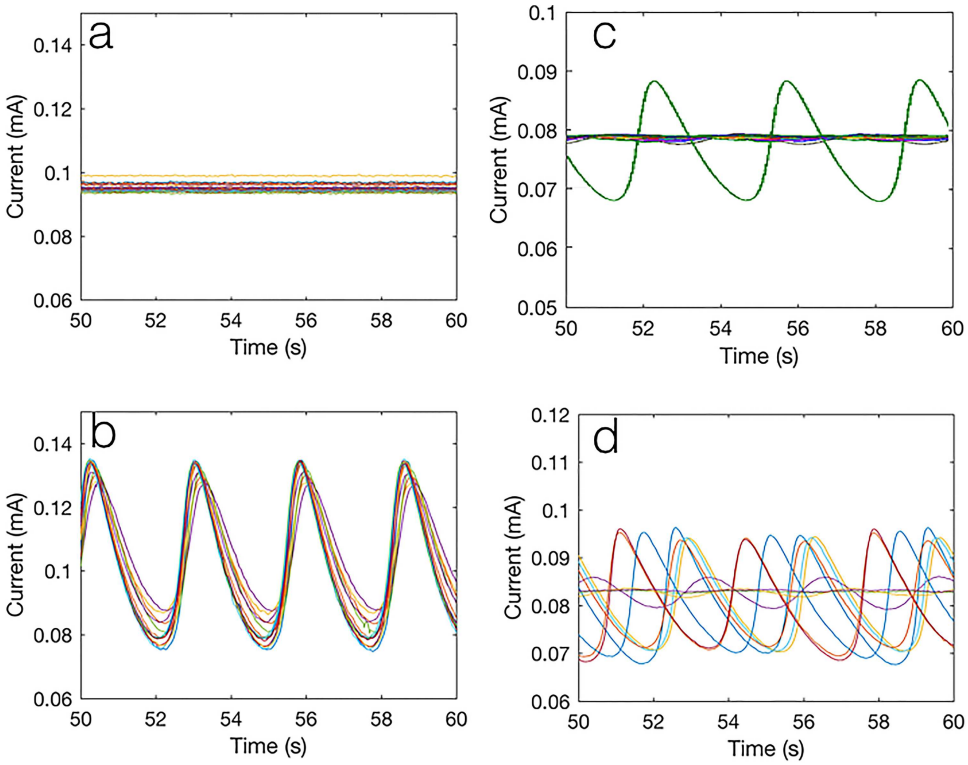

FIG. 2. Experiments: Transition to oscillatory behavior by decreasing N with strong (left) and weak (right) coupling. Current vs time plots. (a) Strong coupling, large population. $N = 40$. $V = 2125$ mV, $R_{ind} = 2.5\,\text{k}\Omega$. (b) Strong coupling, small population. $N = 14$. $V = 2125$ mV, $R_{ind} = 2.5\,\text{k}\Omega$. (c) Weak coupling, large population. $N = 30$. $V = 2650$ mV, $R_{ind} = 10\,\text{k}\Omega$. (d) Weak coupling, small population, $N = 11$. $V = 2650$ mV, $R_{ind} = 10\,\text{k}\Omega$.

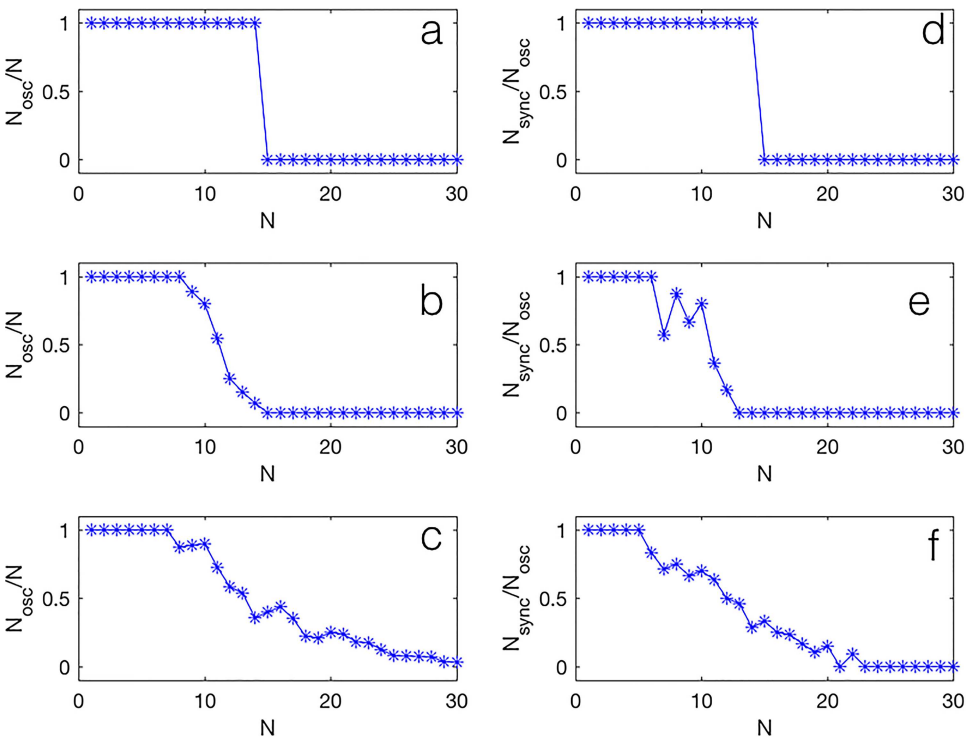

FIG. 3. Experiments: Fraction of oscillating and synchronized electrode currents as a function of number of anodes ("population density") for different values of individual resistances. Left column: Fraction of oscillatory anode current vs. N. Right column: Fraction of synchronized oscillations vs. N. (a) and (d) $V = 2125$ mV, $R_{ind} = 2.5\,\text{k}\Omega$. (b) and (e) $V = 2350$ mV, $R_{ind} = 5\,\text{k}\Omega$. (c) and (f) $V = 2650$ mV, $R_{ind} = 10\,\text{k}\Omega$.

Published under license by AIP Publishing.

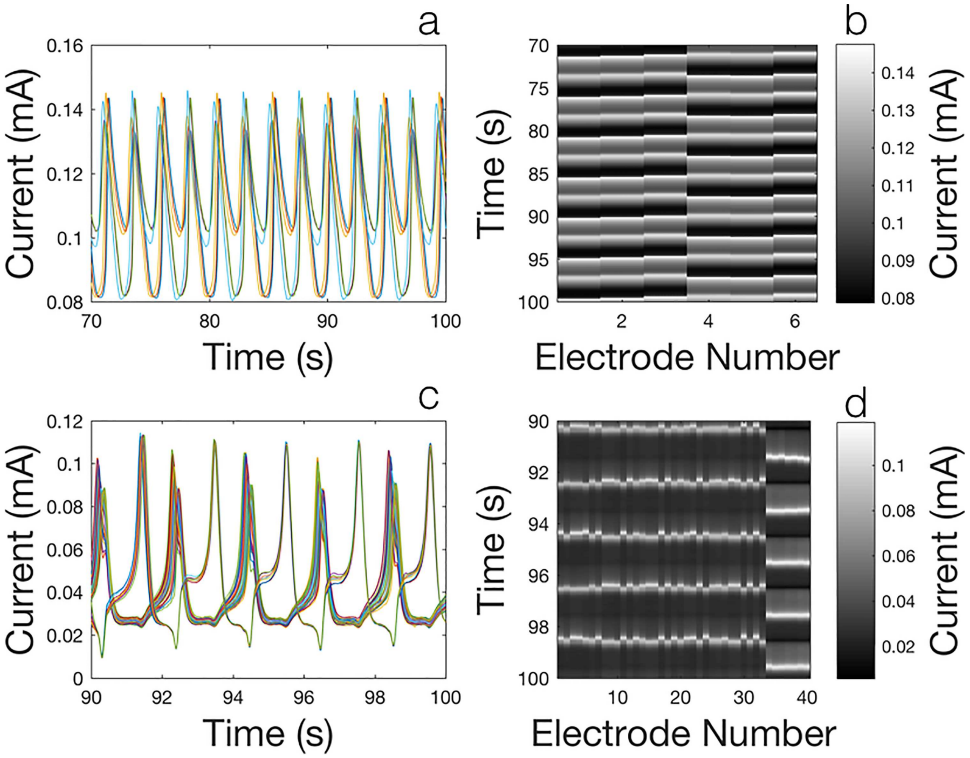

FIG. 4. Experiments: Cluster formation with cathode-anode interactions. Top row: Balanced two-cluster state with $N = 6$. $V = 2230$ mV, $R_{ind} = 500\ \Omega$. (a) Current vs time. (b) Grayscale plot. Bottom row: Unbalanced two-cluster with $N = 40$. $V = 2350$ mV, $R_{ind} = 5$ kΩ. (c) Current vs time. (d) Grayscale plot.

we had seen with the two examples ($R_{\text{ind}} = 2.5$ kΩ and 10 kΩ) above. Some of the currents of the electrodes exhibit oscillations with $N \leq 14$; however, all the electrode currents are not oscillatory until $N = 8$ [Fig. 3(b)]. Furthermore, the oscillations are not fully synchronized until $N = 6$ [Fig. 3(e)].

In addition to the relatively simple, one-cluster synchronization observed at relatively low circuit potentials, stable two-cluster dynamics can also be observed at higher circuit potentials. In Figs. 4(a) and 4(b), the system exhibits two separate groups of period-2 oscillators at $R_{ind} = 500\ \Omega$ with $N = 6$. The grayscale plot further clarifies the presence of balanced cluster configuration with three elements in each clusters. In Figs. 4(c) and 4(d), an unbalanced two-cluster pattern was observed with $N = 40$ close to the homoclinic bifurcation in the system[33] ($R_{ind} = 5$ kΩ).

B. Theory and simulations

To confirm the experimental findings, we developed a model for the cathode-anode interactions in the electrochemical cell. The goal is to show the relationship between the coupling topology in a multiple anode–single cathode electrochemical cell configuration and the quorum sensing type of interactions.

The charge balance in the cathode-anode cell is modeled using the equivalent circuit diagram in Fig. 1(b). At constant circuit potential (V),

$$V = E_k + R_{ind} i_k - E_c, \tag{1}$$

where E_k and i_k are the electrode potential and current, respectively, for anode k (for $k = 1,2,\ldots,N$), E_c is the electrode potential for the cathode, and N is the number of anodes. (We consider the anodic and the cathodic electrode potentials to be positive and negative, respectively.) The currents through the cathode (i_c) and the anodes (i_k) have Faradaic (charge transfer due to chemical reactions) and capacitive (charging) components. Therefore,

$$i_k = A_k j_{F,a}(E_k) + A_k C_{d,a} \frac{dE_k}{dt} \text{ for } k = 1, 2, \ldots, N, \tag{2}$$

$$i_c = A_c j_{F,c}(E_c) + A_c C_{d,c} \frac{dE_c}{dt}, \tag{3}$$

where A_k is the anodic surface area for anode k ($A_k = A_1 = \cdots = A_N$), A_c is the cathodic surface area, and $j_{F,a}(E_k)$ and $j_{F,c}(E_c)$ are the anodic and cathodic Faradaic current densities, which depend on their respective electrode potentials. $C_{d,a}$ and $C_{d,c}$ are the double-layer capacitances per surface areas for the anode and the cathode, respectively. The cathodic current ($i_c < 0$) is the same as the sum of the anodic currents ($i_k > 0$) multiplied by -1

$$i_c = -\sum_{k=1}^{N} i_k. \tag{4}$$

From Eq. (1), we obtain i_k as

$$i_k = \frac{V - E_k + E_c}{R_{ind}} \text{ for } k = 1, 2, \ldots, N. \tag{5}$$

Published under license by AIP Publishing.

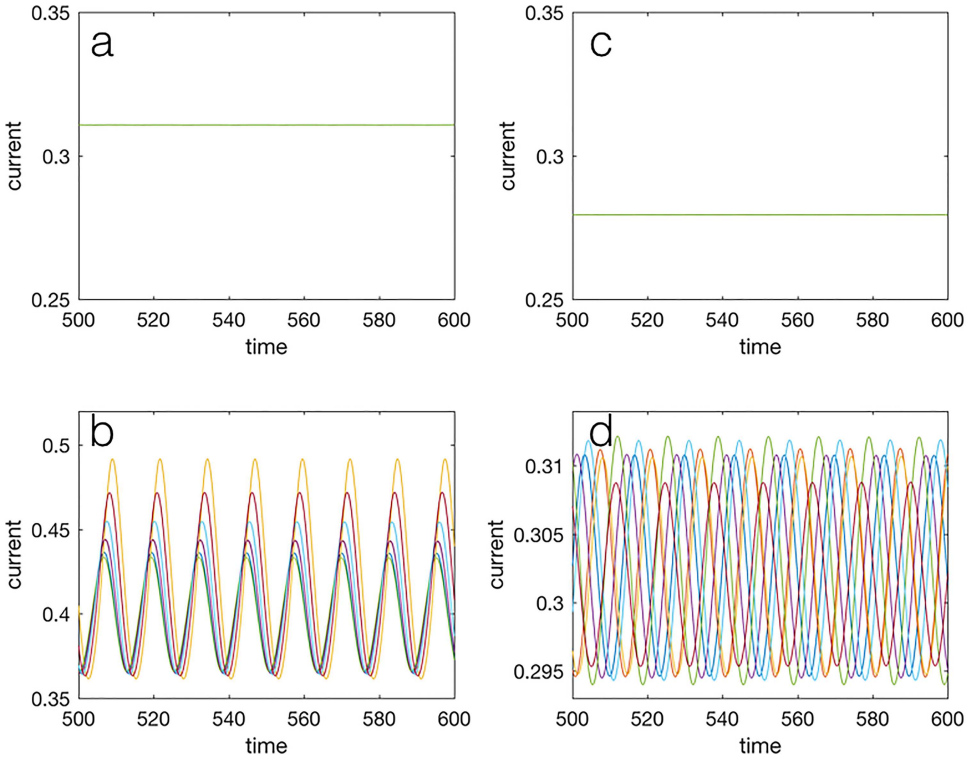

FIG. 5. Simulations: Transition to oscillatory behavior by decreasing N with strong (left) and weak (right) coupling. Current vs. time plots. (a) Strong coupling, large population. $N = 33$. $V = 4.2$, $R_{ind} = 15$, $A_c = 1$, $A_k = 0.5$. (b) Strong coupling, small population. $N = 7$. $V = 4.2$, $R_{ind} = 15$, $A_c = 1$, $A_k = 0.5$. (c) Weak coupling, large population. $N = 33$. $V = 19.3$, $R_{ind} = 70$, $A_c = 1$, $A_k = 0.5$. (d) Weak coupling, small population. $N = 7$. $V = 19.3$, $R_{ind} = 70$, $A_c = 1$, $A_k = 0.5$.

Next, we can rearrange Eqs. (2) and (3) to obtain the ordinary differential equations for the changes of the electrode potentials

$$C_{d,a}\frac{dE_k}{dt} = \frac{V}{A_k R_{ind}} - j_F(E_k) + \frac{(E_c - E_k)}{A_k R_{ind}} \text{ for } k = 1, 2, \ldots, N, \quad (6)$$

$$C_{d,c}\frac{dE_c}{dt} = -\frac{NV}{A_c R_{ind}} - j_F(E_c) + \frac{\left[\left(\sum_{k=1}^{N} E_k\right) - NE_c\right]}{A_c R_{ind}}. \quad (7)$$

Using the mean field approximation for the electrode potentials of the anodes, we can make a substitution for the summation of the anode electrode potentials

$$\bar{E} = \frac{\sum E_k}{N}, \quad (8)$$

$$\bar{E}N = \sum E_k, \quad (9)$$

where $\bar{E}$ is the mean field of the anode electrode potentials. The coupling constants in the last terms of Eqs. (6) and (7) can be combined into parameters K and ρ

$$K = \frac{1}{A_k R_{ind}}, \quad (10)$$

$$\rho = \frac{NA_k}{A_c}. \quad (11)$$

To complete the model, kinetic information is needed for the Faradaic current density in Eqs. (6) and (7). For $j_F(E_c)$, we used Tafel kinetics (the first order reaction with a constant surface concentration of the electroactive species) for the hydrogen ion reduction.[39] For $j_{F,a}(E_k)$, we used a kinetic scheme for Ni electrodissolution,[46] where the Faradaic current density depends on both the electrode potential and the surface coverage of the nickel oxide and hydroxide species (θ)

$$\frac{dE_k}{dt} = \frac{V}{A_k R_{ind}} - \left(\frac{C_h \exp(0.5E_k)}{1 + C_h \exp(E_k)} + \alpha \exp(E_k)\right)(1 - \theta_k) + K(E_c - E_k) \text{ for } k = 1, 2, \ldots N, \quad (12)$$

$$\frac{d\theta_k}{dt} = \frac{1}{\Gamma_k}\left[\frac{\exp(0.5E_k)}{1 + C_h \exp(E_k)}(1 - \theta_k) - \frac{\beta C_h \exp(2E_k)}{\gamma C_h + \exp(E_k)}\theta_k\right] \text{ for } k = 1, 2, \ldots, N, \quad (13)$$

$$\sigma\frac{dE_c}{dt} = \frac{-NV}{A_c R_{ind}} - j_0 \exp[-0.5(E_c - E_{c0})] + \rho K(\bar{E} - E_c), \quad (14)$$

where $C_h = 1600$ is the hydrogen ion concentration, $\alpha = 0.3$, $\beta = 6 \times 10^{-5}$, $\gamma = 0.001$ are kinetic constants, $j_0 = -1$ is the exchange current density, $E_{C0} = 0$ is the open circuit potential of the cathode, Γ_k are the surface capacities of the oxide and hydroxide species, $\sigma = 1$ is the (relative) cathode double layer capacitance). (Note that following the original rescaling,[39] the equations are in dimensionless forms.) In the experiments, there are always some small differences in the surface conditions, which, for example, result in a distribution

Published under license by AIP Publishing.

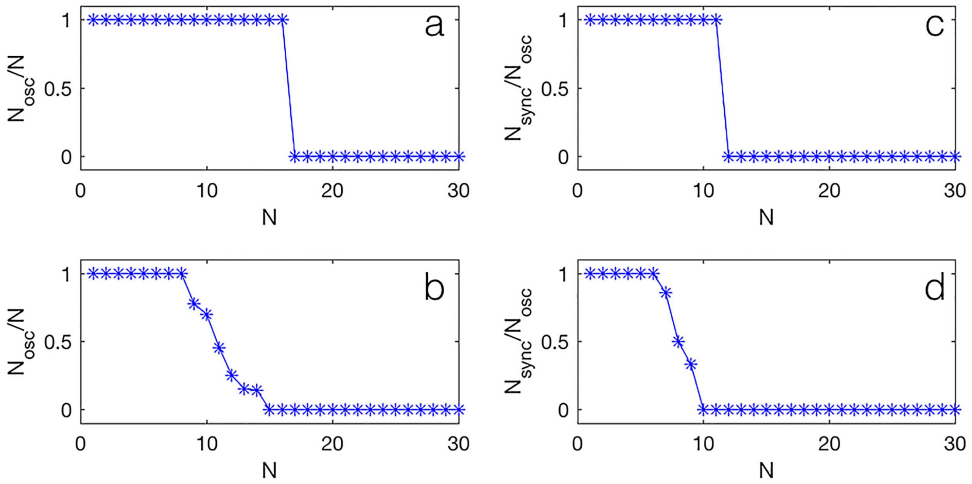

FIG. 6. Simulations: Fraction of oscillating and synchronized electrode currents as a function of the number of anodes ("population density") for different values of individual resistances. Left column: Fraction of oscillatory anode current vs. N. Right column: Fraction of synchronized oscillations vs. N. (a) and (c) $V = 4.2$, $R_{ind} = 15$, $A_c = 1$, $A_k = 0.5$. (b) and (d) $V = 12.7$, $R_{ind} = 50$, $A_c = 1$, $A_k = 0.5$.

of the natural frequency of the oscillations.[45] The surface capacities (Γ_k) were set to a normal random distribution with mean and standard deviation of 0.01 and 1×10^{-4}, respectively; the random distribution aims to simulate the inherent surface heterogeneities of the electrodes.[45]

The electrochemical model equations were numerically integrated, starting with $N = 33$ and decreasing N similar to the experimental procedure. (In this set of simulations the transitions were observed well below $N = 40$, therefore, we started at $N = 33$.) With $N = 33$, at low external resistance, $R_{ind} = 15$, the currents are stationary [see Fig. 5(a)]. As N was decreased, the currents remained stationary [see Fig. 6(a)], until $N = 16$, where all the electrodes exhibited synchronized oscillations [see Fig. 6(c)]. The synchronized oscillations for $N = 7$ are shown in Fig. 5(b). Therefore, at low R_{ind}, the simulation agreed with experiments in showing abrupt transition to synchronized oscillations with decreasing N.

At higher external resistance ($R_{ind} = 70$), we see a gradual transition [see Figs. 6(b) and 6(d)] from a stationary state [$N = 33$, Fig. 5(c)] to partially synchronized oscillations [$N = 7$, Fig. 5(d)]; the oscillations became fully synchronized only with $N = 6$. Therefore, the model also reproduced that at higher individual resistances the transition to oscillations is more gradual, and full synchrony occurs at smaller N, than that needed at lower R_{ind}.

At larger V (closer to homoclinic bifurcation), clustering behavior can be observed with the model simulations as well. Figures 7(a) and 7(b) show the current vs. time for the oscillatory electrode potentials at $V = 35.1$ and $R_{ind} = 50$, $N = 40$. Two-cluster behavior is observed, where the oscillations have the same frequency (0.0565 Hz); in each cluster the oscillations are nearly in-phase, but elements in the two clusters oscillate in nearly anti-phase configurations.

The experimental and numerical findings can be qualitatively explained by the star topology of the coupling (schematically shown in Figure 8) as defined by Eqs. (12)–(14). The cathode is coupled to all the anodes with coupling strength $K = 1/(A_k R_{ind})$. At low R_{ind} the coupling is strong, at large R_{ind} the coupling is weak. The anodes are coupled to the cathode with coupling strength ρK, where ρ is proportional to the number of anodes [Eq. (11)]. The cathode mediates the coupling among the anodes, and the mathematical formula for the coupling mechanism is equivalent to dynamical quorum sensing:[22] The active oscillators contribute to the mean field of the "medium" (cathode) through mixing, and the medium (cathode) is coupled to the behavior of the active elements. However, in contrast to the often assumed "passive" medium, the cathode has an important source, the Faradaic current density, that can adjust the cathode potential while the coupling is being mediated. For synchronized oscillations

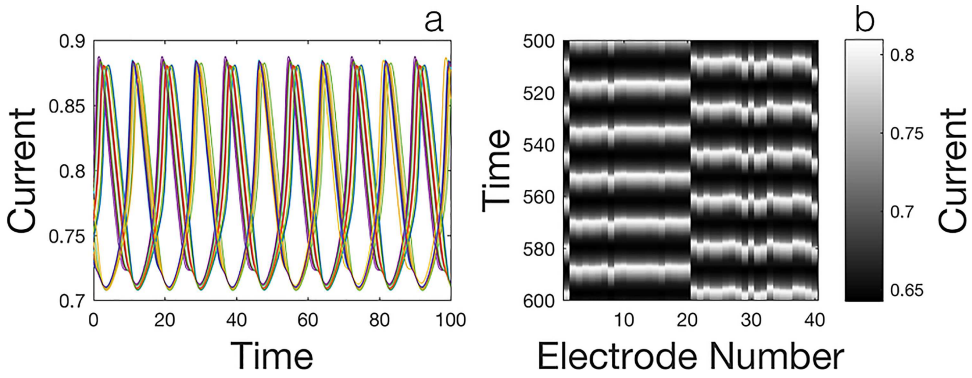

FIG. 7. Simulations: Cluster formation due to cathode-anode interactions. (a) Current vs. time and (b) Grayscale plot. $N = 40$, $V = 35.1$, $R_{ind} = 50$. $A_c = 1$, $A_k = 0.5$.

Published under license by AIP Publishing.

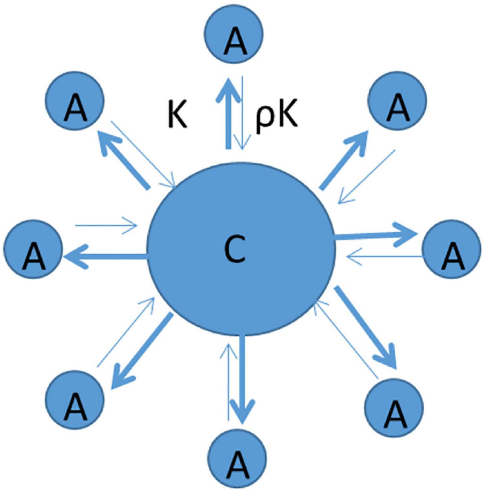

FIG. 8. Global coupling topology expressed by the single-cathode, multi-anode nickel dissolution system. The coupling strength, K, is dependent on the size of each anode and the individual resistance [Eq. (10)]. The population density term, ρ, is determined by the number of all anodes connected to the system (N) and the ratio of the surface areas of the individual anode and the cathode [Eq. (11)].

to occur, one would expect sufficiently strong coupling (K and ρ). Additionally, the cathode potential directly enters the anode potential equations; in general, the anode potential can be quite different from the cathode potentials. As the number of anode wires are changed, the cathodic potential is adjusted to provide the cell current. With the coupling term in Eq. (14), an offset signal is transmitted to the anodes, which can change the bifurcation parameters for the oscillations. The composite effect of the coupling thus can result in the emergence of synchronized or desynchronized oscillations, depending on the coupling strength and the extent of heterogeneities in the system.

V. CONCLUSIONS

We showed that in a multi-particle anode–single cathode electrochemical system, the electrical interactions can be described with similar mathematical formalism to quorum sensing. This would allow an electrochemical system to sense the number of anodes and, by design, to change the dynamical behavior in response to changing the anode number. In the given system, in which the conditions were set slightly below a Hopf bifurcation for a large population, with decreasing the number of anodes ("population density"), a transition occurs to oscillations. The oscillations are thus observed with a decreasing population density, and an "inverse" dynamical quorum transition takes place. While the occurrence of oscillations with decreasing population density is different from some of the earlier observations,[18,24] theoretical models[47] have predicted such transitions, that were later confirmed with coupled Chua's circuits.[29] (In addition, at very large cell density, the glycolytic oscillations also cease.[17]) Our results show that in the electrochemical system, such transition can occur with the multi-electrode anode and single cathode. We further note that we also performed experiments at very large circuit potential, above the homoclinic bifurcation, where the anodes have excitable behavior. In this case, we observed the onset of oscillations with increasing population density.

With sufficiently strong coupling, the oscillations can occur in a synchronous manner. With weak coupling, the transition is gradual. These two different types of transition confirm theoretical predictions with (chaotic) Rössler oscillators[23] and also similar to the BZ bead experiments.[7] In addition, with very strong coupling, the synchronized behavior can exhibit phase clusters. The rich quorum sensing (or crowd synchrony) transition dynamics observed in our work could have importance in biological systems, e.g., in the vasoactive intestinal peptide (VIP) mediated synchronization of circadian oscillators, where only a small fraction of cells generate sustained oscillations without coupling, but in the presence of coupling a robust, fully synchronized gene expression pattern can be recorded.[48]

ACKNOWLEDGMENTS

I.Z.K. would like to thank Ken Showalter for inspiring discussion about pattern formation in chemical systems and for his support and encouragement. V.G. is grateful to Ken Showalter for lifelong support and friendship both in the professional arena and at the personal level. We also thank Ken Showalter for his mentoring of young scientists that resulted in a lasting impact on Hungarian science in the field of chemical nonlinear dynamics. This material is based upon the work supported by the National Science Foundation under Grant No. CHE-1465013. V.G. acknowledges the support of the National Research, Development and Innovation Fund No. 119360.

REFERENCES

[1] A. T. Winfree, *The Geometry of Biological Time* (Springer, 2001).
[2] A. Pikovsky, M. Rosenblum, and J. Kurths, *Synchronization A Universal Concept in Nonlinear Sciences* (Cambridge University Press, Cambridge, UK, 2001).
[3] Y. Kuramoto, *Chemical Oscillations, Waves and Turbulence* (Springer, Berlin, 1984).
[4] I. Z. Kiss, Y. Zhai, and J. L. Hudson, "Emerging coherence in a population of chemical oscillators," Science **296**(5573), 1676–1678 (2002).
[5] D. K. Verma, H. Singh, P. Parmananda, A. Contractor, and M. Rivera, "Kuramoto transition in an ensemble of mercury beating heart systems," Chaos **25**(6), 064609 (2015).
[6] W. Wang, I. Z. Kiss, and J. L. Hudson, "Clustering of arrays of chaotic chemical oscillators by feedback and forcing," Phys. Rev. Lett. **86**(21), 4954–4957 (2001).
[7] A. F. Taylor, M. R. Tinsley, F. Wang, Z. Y. Huang, and K. Showalter, "Dynamical quorum sensing and synchronization in large populations of chemical oscillators," Science **323**(5914), 614–617 (2009).
[8] A. F. Taylor, M. R. Tinsley, and K. Showalter, "Insights into collective cell behaviour from populations of coupled chemical oscillators," Phys. Chem. Chem. Phys. **17**(31), 20047–20055 (2015).
[9] L. Perié, J. Aru, P. Kourilsky, and J.-J. Slotine, "Does a quorum sensing mechanism direct the behavior of immune cells?," C. R. Biol. **336**(1), 13–16 (2013).
[10] J. Engebrecht, K. Nealson, and M. Silverman, "Bacterial bioluminescence: Isolation and genetic analysis of functions from *Vibrio fischeri*," Cell **32**(3), 773–781 (1983).
[11] A. L. Schaefer, B. L. Hanzelka, A. Eberhard, and E. Greenberg, "Quorum sensing in *Vibrio fischeri*: Probing autoinducer-LuxR interactions with autoinducer analogs," J. Bacteriol. **178**(10), 2897–2901 (1996).
[12] M. G. Surette, M. B. Miller, and B. L. Bassler, "Quorum sensing in *Escherichia coli*, *Salmonella typhimurium*, and *Vibrio harveyi*: A new family of genes responsible for autoinducer production," Proc. Natl. Acad. Sci. **96**(4), 1639–1644 (1999).
[13] J. Mainil, "*Escherichia coli* virulence factors," Vet. Immunol. Immunopathol. **152**(1), 2–12 (2013).

Published under license by AIP Publishing.

[14]Z. Zhang, "Mathematical model of a bacteria-immunity system with the influence of quorum sensing signal molecule," J. Appl. Math. Phys. **4**(05), 888 (2016).
[15]B. O. Emerenini, B. A. Hense, C. Kuttler, and H. J. Eberl, "A mathematical model of quorum sensing induced biofilm detachment," PLoS ONE **10**(7), e0132385 (2015).
[16]A. Sokolov, I. S. Aranson, J. O. Kessler, and R. E. Goldstein, "Concentration dependence of the collective dynamics of swimming bacteria," Phys. Rev. Lett. **98**(15), 158102 (2007).
[17]J. Aldridge and E. K. Pye, "Cell density dependence of oscillatory metabolism," Nature **259**, 670 (1976).
[18]S. Dano, P. Sorensen, and F. Hynne, "Sustained oscillations in living cells," Nature **402**(6759), 320–322 (1999).
[19]A. Weber, Y. Prokazov, W. Zuschratter, and M. J. Hauser, "Desynchronisation of glycolytic oscillations in yeast cell populations," PLoS ONE **7**(9), e43276 (2012).
[20]T. Amemiya, K. Obase, N. Hiramatsu, K. Itoh, K. Shibata, M. Takinoue, T. Yamamoto, and T. Yamaguchi, "Collective and individual glycolytic oscillations in yeast cells encapsulated in alginate microparticles," Chaos **25**, 064606 (2015).
[21]J. Garcia-Ojalvo, M. B. Elowitz, and S. H. Strogatz, "Modeling a synthetic multicellular clock: Repressilators coupled by quorum sensing," Proc. Natl. Acad. Sci. **101**(30), 10955–10960 (2004).
[22]S. De Monte, F. d'Ovidio, S. Danø, and P. G. Sørensen, "Dynamical quorum sensing: Population density encoded in cellular dynamics," Proc. Natl. Acad. Sci. **104**(47), 18377–18381 (2007).
[23]B.-W. Li, C. Fu, H. Zhang, and X. Wang, "Synchronization and quorum sensing in an ensemble of indirectly coupled chaotic oscillators," Phys. Rev. E **86**(4), 046207 (2012).
[24]M. R. Tinsley, A. F. Taylor, Z. Huang, and K. Showalter, "Emergence of collective behavior in groups of excitable catalyst-loaded particles: Spatiotemporal dynamical quorum sensing," Phys. Rev. Lett. **102**(15), 158301 (2009).
[25]R. Toth, A. F. Taylor, and M. R. Tinsley, "Collective behavior of a population of chemically coupled oscillators," J. Phys. Chem. B. **110**(20), 10170–10176 (2006).
[26]S. H. Strogatz, D. M. Abrams, A. Mcrobie, B. Eckhardt, and E. Ott, "Theoretical mechanics: Crowd synchrony on the Millennium Bridge," Nature **438**(7064), 43–44 (2005).
[27]J. Zamora-Munt, C. Masoller, J. Garcia-Ojalvo, and R. Roy, "Crowd synchrony and quorum sensing in delay-coupled lasers," Phys. Rev. Lett. **105**(26), 264101 (2010).
[28]H. Singh and P. Parmananda, "Crowd synchrony in chaotic oscillators," Nonlinear Dyn. **80**(1–2), 767–776 (2015).
[29]H. Singh and P. Parmananda, "Quorum sensing via static coupling demonstrated by Chua circuits," Phys. Rev. E. **88**, 040903(R) (2013).
[30]T. Singla, F. Montoya, M. Rivera, S. Tajima, S. Nakabayashi, and P. Parmananda, "Synchronization using environmental coupling in mercury beating heart oscillators," Chaos **26**(6), 063103 (2016).
[31]T. Danino, O. Mondragón-Palomino, L. Tsimring, and J. Hasty, "A synchronized quorum of genetic clocks," Nature **463**(7279), 326–330 (2010).
[32]W. Wang, I. Z. Kiss, and J. L. Hudson, "Experiments on arrays of globally coupled chaotic electrochemical oscillators: Synchronization and clustering," Chaos **10**(1), 248–256 (2000).
[33]I. Z. Kiss, Y. Zhai, and J. L. Hudson, "Predicting mutual entrainment of oscillators with experiment-based phase models," Phys. Rev. Lett. **94**(24), 248301 (2005).
[34]I. Z. Kiss, C. G. Rusin, H. Kori, and J. L. Hudson, "Engineering complex dynamical structures: Sequential patterns and desynchronization," Science **316**(5833), 1886–1889 (2007).
[35]M. Wickramasinghe and I. Z. Kiss, "Spatially organized partial synchronization through the chimera mechanism in a network of electrochemical reactions," Phys. Chem. Chem. Phys. **16**(34), 18360–18369 (2014).
[36]M. Wickramasinghe and I. Z. Kiss, "Spatially organized dynamical states in chemical oscillator networks: Synchronization, dynamical differentiation, and chimera patterns," PLoS ONE **8**(11), e80586 (2013).
[37]Y. Jia and I. Z. Kiss, "Spontaneously synchronized electrochemical microoscillators with nickel electrodissolution," J. Phys. Chem. C **116**(36), 19290–19299 (2012).
[38]M. Wickramasinghe and I. Z. Kiss, "Nonlinear behavior of nickel dissolution in sulfuric acid in a cathode-anode cell configuration: Effect of cathode area," J. Electrochem. Soc. **163**(14), H1171–H1178 (2016).
[39]M. J. Hankins, M. Wickramasinghe, and I. Z. Kiss, "Synchronization of current oscillations in a dual-anode dissolution reaction in the presence of a common cathode electrode," Electrochim. Acta **252**, 76–83 (2017).
[40]M. G. T. Fechner, "Ueber Umkehrungen de Polarität in der einfachen Kette," J. Chemie Physik **53**, 129 (1828).
[41]V. Petrov, V. Gáspár, J. Masere, and K. Showalter, "Controlling chaos in the Belousov-Zhabotinsky reaction," Nature **361**(6409), 240–243 (1993).
[42]I. Z. Kiss, V. Gaspar, L. Nyikos, and P. Parmananda, "Controlling electrochemical chaos in the copper-phosphoric acid system," J. Phys. Chem. A **101**, 8668–8674 (1997).
[43]I. Z. Kiss, V. Gaspar, and J. L. Hudson, "Experiments on synchronization and control of chaos on coupled electrochemical oscillators," J. Phys. Chem. B **104**, 7554–7560 (2000).
[44]I. Z. Kiss, Z. Kazsu, and V. Gáspár, "Tracking unstable steady states and periodic orbits of oscillatory and chaotic electrochemical systems using delayed feedback control," Chaos **16**(3), 033109 (2006).
[45]I. Z. Kiss, W. Wang, and J. L. Hudson, "Experiments on arrays of globally coupled periodic electrochemical oscillators," J. Phys. Chem. B **103**(51), 11433–11444 (1999).
[46]D. Haim, O. Lev, L. M. Pismen, and M. Sheintuch, "Modeling periodic and chaotic dynamics in anodic nickel dissolution," J. Phys. Chem. **96**(6), 2676–2681 (1992).
[47]H. Singh and P. Parmananda, "Alternate coupling mechanism for dynamical quorum sensing," J. Phys. Chem. A **116**(42), 10269–10275 (2012).
[48]T.-L. To, M. A. Henson, E. D. Herzog, and F. J. Doyle, "A molecular model for intercellular synchronization in the mammalian circadian clock," Biophys. J. **92**(11), 3792–3803 (2007).

Published under license by AIP Publishing.